Fully Automated Annotation of Seismocardiogram for Noninvasive Vital Sign Measurements

Niccolò Mora, Federico Cocconcelli, Guido Matrella, and Paolo Ciampolini

***Abstract*— This paper presents a fully automated procedure for acquiring and analyzing seismocardiographic (SCG) traces from an inertial measurement unit (IMU) placed over a subject's sternum. An automated calibration procedure allows for straightforward adaption to different subjects. Calibration is performed once per subject, exploiting electrocardiogram (ECG) markers; relevant patterns and parameters are automatically extracted and used for successive SCG processing, which does not require concurrent ECG information any longer. Annotation of SCG traces is performed in two steps: in the first one, a suitably engineered signal is derived from SCG and used as coarse heartbeat detector; then, the annotation can be performed by comparing the prototype extracted at calibration time with segments of SCG data, near to the detected beats. The proposed methodology is validated by direct comparison with ECG, adopted as gold standard. In particular, three main metrics are taken into account: sensitivity (i.e., the percentage of correctly identified heartbeats, compared to ECG), precision (i.e., impact of false positives on truly detected beats), and R^2 (i.e., linearity between beat-to-beat measurements as computed by ECG and SCG). Results show satisfactory performance, more than adequate to continuous, long-term monitoring: overall, approximately 90% of heartbeats are correctly detected, on average, with minimal false positives ($\approx 1\%$). Linearity between ECG- and SCG-computed beat-to-beat intervals is extremely high ($R^2 > 0.95$, on average), indicating good agreement between the two measurement methods. These results suggest that SCG can be used as a reliable, contactless measure of heart-related parameters.**

***Index Terms*— Accelerometry, active assisted living (AAL), inertial measurement unit (IMU), seismocardiogram (SCG), vital sign monitoring.**

I. Introduction

INFORMATION and communication technologies (ICT) is a key asset for active and healthy aging (A&HA). For example, smart living environments may allow older persons to stay longer and better in their own home, by providing home automation [1] and collaborative services [2]. Smart environments may also improve personal safety: for example, environmental sensors may be used to detect nighttime wandering events in homes of older adults suffering from Alzheimer's disease [3]. Further active and ambient assisted living (AAL [4]) techniques may help in making services more accessible by compensating physical impairments with new smart devices. For examples, brain–computer interfaces have been integrated within AAL systems to allow severely motor-impaired users to achieve communication and home control [5], [6]. Smart objects and Internet of Things (IoT) technology also enable long-term behavioral monitoring, which analyzes behavioral features for indirectly probing user's wellbeing: for instance, behavioral patterns can be discovered from common home environmental sensors [7]. Behavioral changes over different periods or subjects, or the emergence of new trends (possibly correlated with health issues) can be detected and made known to caregivers, significantly enhancing their insight. Activities of daily living (ADL) can be recognized and traced as well [8], providing useful information on subjects' routines and self-sufficiency. To allow for effectiveness and sustainability, supportive technologies need to be inexpensive and accessible. They have to be perceived as noninvasive and minimally intrusive, so that they do not interfere with daily living habits. In a data fusion perspective, behavioral monitoring can be effectively complemented by vital signs monitoring as well, providing a more comprehensive and accurate vision, with vital sign monitors being subject to the same ergonomic and economic constraints just mentioned. Within the wide spectrum of vital sign measurements, acquired in daily-life scenarios, cardiovascular signals are by far the most targeted. For example, continuous monitoring of heart rate (HR) and HR variability (HRV, defined as the standard deviation of beat-to-beat intervals) can be achieved exploiting many different techniques: electrocardiography (ECG) is the primary measurement method for such quantities [9]. Besides clinical applications, such as automated heart condition classification [10], or full day recording of heart activity by means of Holter devices, many consumer-grade HR monitors (e.g., fitness chest strap) measure the electrical potentials from a single ECG lead. However, prolonged contact of electrodes with the skin may cause irritation and wear, causing discomfort and hindering the possibility to carry out daily, continuous monitoring. Another popular technique, exploited by most wrist-worn monitors, is photoplethysmography (PPG). PPG senses light absorption variations, in distal locations, due to an increased/decreased presence of oxyhemoglobin carried by a blood pulse. Thus, HR measurements are immediately derived; by exploiting different wavelength light sources, peripheral oxygen saturation (SpO_2) can be measured as well [11]. With PPG, prolonged use may cause skin irritation due to heating from the light source. Besides HR, PPG has also been used to derive measurements of respiration [12].

Manuscript received December 4, 2018; revised February 1, 2019; accepted March 8, 2019. Date of publication April 1, 2019; date of current version March 10, 2020. The Associate Editor coordinating the review process was Sabrina Grassini. *(Corresponding author: Niccolò Mora.)*

The authors are with the Dipartimento di Ingegneria e Architettura, Università degli Studi di Parma, 43121 Parma, Italy (e-mail: niccolo.mora@unipr.it; federico.cocconcelli@unipr.it; gudido.matrella@unipr.it; paolo.ciampolini@unipr.it).

Color versions of one or more of the figures in this article are available online at http://ieeexplore.ieee.org.

Digital Object Identifier 10.1109/TIM.2019.2908511

Such measures can also be obtained remotely, without direct body contact, by exploiting the Doppler radar measurement systems [13], [14] or millimeter-wave antennas [15]; however, these systems are not suitable for daily use, as they involve complex setups. Finally, blood pressure measurements are largely targeted within the realm of vital sign monitoring. Besides automated sphygmomanometers, indirect measurement techniques have been devised based on the measurement of pulse transit time (PTT), i.e., the time that takes for the blood pressure wave to travel from a proximal point to a distal one in the arterial tree within the same cardiac cycle. Such measurement can be performed, for example, by taking PPG as distal location reference and ECG as proximal one [16].

Recent improvements in performance and cost-effectiveness of microelectro-mechanical systems (MEMS) devices have opened new possibilities in continuous vital sign monitoring. Accelerometers and inertial measurement units (IMUs) can be leveraged to measure vibrations produced by the heart mechanical activity. In particular, ballistocardiography (BCG) and seismocardiography (SCG) are promising techniques to extract information on cardiac events and phases, including mentioned HR and HRV indicators. Compared to ECG and PPG, such techniques have the advantage of not requiring any contact electrode or detector: the sensing element can be secured in place by a fixture, without direct access to exposed skin; this may prevent irritations, allowing for much longer monitoring sessions. With such a continuous monitoring perspective, it is also important to mention the possibility of exploiting the very same accelerometric device for multiple measurements to jointly assess heart parameters and physical activity indicators, thus providing contextualized and much more expressive information. It could be possible to acquire information such as step count, energy expenditure, quality of movement (e.g., symmetry in gait), and many others. Also, accelerometer features may be fused with home environment sensors to achieve improved ADL detection, thus contributing to a more general and ubiquitous AAL monitoring framework.

This paper focuses on the development of an automatic procedure for acquiring SCG waveforms and identifying its characteristic points, directly related to specific heart cycle phases. The methodology is validated by direct comparison with ECG information, adopted as gold standard. Note that, except for a quick calibration phase (only required if detailed SCG annotation is desired), the relevant measures can be directly computed from the SCG traces alone; furthermore, such phase is carried out just once per subject. The results achieved, in terms of heartbeat detection, false-positive immunity, and agreement with ECG-based reference intervals shows that the proposed method reliably extracts HR information.

II. Methods

A. Related Work

SCG [17] is the study of the precordial vibrations produced by the cardiac contractions and by the mass of the blood ejected from the ventricles. SCG has been known for decades, but only the recent technological advancements in low-noise, low-power IMU has allowed to perform precise, long-term readings of such signal [18], [19]. At the same time, different methodologies for cardiac events detection have been proposed based on vibrational studies. For example, BCG measures whole-body vibrations in response to cardiac activity and blood ejection. It can be acquired noninvasively, for instance, by means of load cells in weight scales [20] or piezoelectric films between the subject and the bed [21]. On the other hand, *Gyrocardiography* (GCG) [22] can provide similar information to SCG, by capturing the rotational movement of the chest wall. Finally, phonocardiography (PCG) records high-definition heart sounds, which arise from the cardiac activity: recently, deep-learning techniques have been devised to analyze and classify such signals [23], for detecting pathological conditions. Also, PCG devices (similar to PPG mentioned earlier) may act as proximal point detector [24], complementing ECG in order to estimate PTTs during cuff-less blood pressure monitoring measurements.

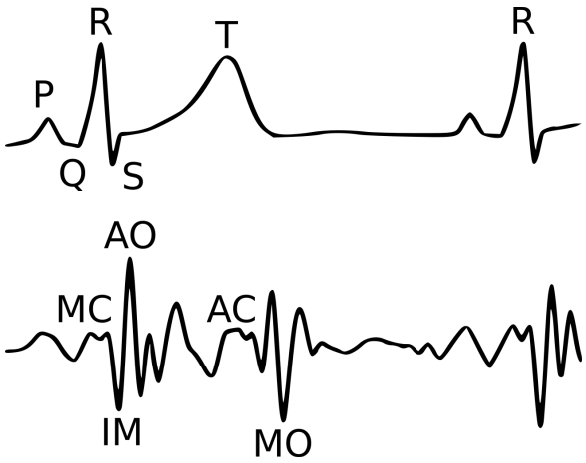

Fig. 1. Correlation between ECG and SCG waveforms, with their annotated characteristic landmarks.

Fig. 1 shows the relationship between the hearts electrical activity, measured with ECG and the SCG signal. Five landmarks are identified, strictly related to cardiac mechanics: mitral valve closure (MC), isovolumic moment (IM), aortic valve opening (AO), aortic valve closure (AC), and mitral valve opening (MO). In order to acquire a stable SCG, the IMU is usually placed on the subject's chest, typically over the sternum: this position allows to acquire good amplitude signals; furthermore, it has the advantage of being along the vertical symmetry axis, therefore, the sensing element can also be repurposed to evaluate motion symmetry.

Many works in the literature [25]–[27] focused on automated recognition of relevant peaks and patterns, in order to derive systolic time intervals measurements, such as HR, HRV, preejection period (PEP), and left ventricle ejection time (LVET). In most cases, such detection is performed by exploiting the dorsoventral axis of the accelerometer data. Some heart conditions can be monitored exploiting SCG: for example, Salerno and Zanetti [28] were able to quantitatively evaluate changes in left ventricular function during an ischemic episode. Other works describe methodologies to detect atrial fibrillation by means of joint time–frequency analysis of SCG traces [29] or focus more on a portable implementation, exploiting mobile phones [30].

With respect to the literature work, this paper mostly focuses on developing a fully automatic procedure for the acquisition and annotation of the SCG traces. This is to be framed in the development of a low-cost, wearable device, suitable for multidimensional (i.e., heart and activity) monitoring and for deployment in practical AAL environments [31], [32]. For usability's sake, fully automated calibration procedures are introduced. Beat detection can be self-consistently calibrated, by focusing on certain detection signal features. If a more detailed annotation of further SCG signal features is needed, concurrent ECG measurement can be exploited to provide a reliable reference, according to the automated procedure described in the following. Nonetheless, calibration needs to be performed just once per subject, and after full calibration, user-specific assessment is carried out in an "unsupervised" fashion, i.e., without further need of concurrent ECG information.

B. Measurement Protocol and Data Acquisition

Fifteen acquisitions were performed for this paper, involving healthy subjects without any documented history of cardiac problems; all participants volunteered for this study, conducted following the guidelines of the Helsinki declaration on ethical principles. Each session, lasting about 3 min, consisted in the simultaneous acquisition of the SCG and, for validation purposes, of the ECG. Subjects were comfortably sitting on a chair while measurements were being taken. The experimental setup for data capture involved four main units: an SCG acquisition device, an ECG analog front end (AFE), a microcontroller unit (MCU) to synchronize and control field-data acquisition, and a desktop PC to collect data and analyze them at a later stage.

SCG signals were acquired by means of a MEMS IMU; namely, an ST Microelectronics LSM6DS33 device was exploited. In order to achieve electrical insulation and to allow a more stable placement of the accelerometer sensor, the IMU board was enclosed in a small plastic container (approximately $40 \times 25 \times 15$ mm^3). The fixture was then positioned over the subject's sternum and secured in place using a belt and medical tape (ergonomic design of the wearable device will be taken care of at a later stage). The orientation of the IMU device is such that the $\{x, y\}$ plane is parallel to the chest wall (with the x-axis parallel to the right-to-left shoulder direction, and the y-axis parallel to the foot-to-head direction), whereas the z-axis is perpendicular to it (i.e., parallel to the dorsoventral direction). For the present study, without any loss in generality, analysis of the SCG is restricted just to the dorsoventral direction. The experimental setup is sketched in Fig. 2. As far as the IMU parameter setup is concerned, the device was set to operate at a sensitivity of 61 μg/LSB ($g \approx 9.81$ m/s^2), featuring a full dynamic range of ± 2 g; antialias filtering is performed on-chip, with a 50-Hz cutoff frequency. Data reading and management of the IMU sensor is handled by the MCU, exploiting the interintegrated circuit (I2C) serial protocol for data transfer.

Besides SCG, the reference ECG signal is simultaneously acquired, using standard Ag/AgCl electrodes. A standard lead-I ECG is recorded from the right arm and left arm

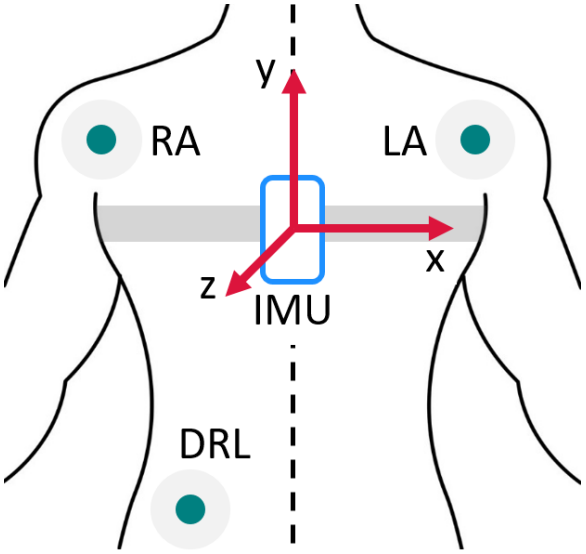

Fig. 2. Positioning of IMU sensor and ECG electrodes. The IMU is placed over the subject's sternum, with the reference system as shown by the $\{x, y, z\}$-axes. A standard ECG lead-I is formed by LA–RA electrodes, whereas the DRL electrode provides attenuation of 50-Hz common mode noise.

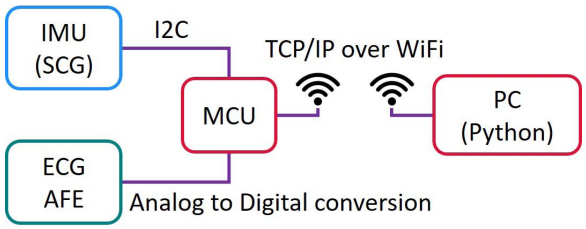

Fig. 3. Block diagram of the synchronous SCG–ECG acquisition system, handled by an MCU; measurement data are streamed via Wi-Fi, exploiting TCP/IP protocol. A desktop PC is used for data logging and subsequent processing.

electrode sites (or RA–LA in Fig. 2). The acquired signal is amplified by means of an analog devices AD8232 IC, which provides a low-noise, ac-coupled 40-dB gain instrumentation amplifier (INA); a second-order Sallen–Key low-pass filter is then cascaded to the INA, providing further 20 dB of dc gain and a rolloff of -40 dB/dec from the cutoff frequency at 40 Hz onward. Furthermore, in order to reduce the effect of electromagnetic interference coupling from mains (220 V, 50 Hz) through the body, a right leg driver feedback circuit is added, providing up to 26-dB loop gain for the rejection of 50-Hz common mode noise. Finally, the signal is digitalized by exploiting a 12-bit analog-to-digital converter (ADC) on the MCU.

Both SCG and ECG signals were sampled at 100 samples per second (SPS). The acquisition is performed synchronously by means of an ARM Cortex M0+ MCU. Incoming data are buffered and sent into bursts, in order to maximally exploit the Wi-Fi (IEEE 802.11 b/g/n) TCP/IP connectivity. Real-time data logging is achieved at the receiving side by the implementation of a Python TCP client, running on a standard desktop PC. Data curation and analysis is carried out in the same environment, exploiting NumPy and SciPy packages. The complete measurement system is sketched as a block diagram in Fig. 3.

Before applying further analyses, data are preprocessed: ECG signals are filtered over a (0.1–35 Hz) passband, whereas IMU accelerometer data are bandpass filtered over a (4–20 Hz) band. Filters were designed exploiting Kaiser window finite impulse response (FIR) filter design. In order to maintain the phase relationship between filtered SCG and ECG signals, the zero-phase digital filtering mode is exploited. In addition, to account for different, subject-specific, signal amplitudes, data are scaled by means of *z-scoring*

$$x_z = \frac{x - \mu_x}{\sigma_x} \tag{1}$$

where x is the signal of interest, μ_x is its mean, and σ_x is the standard deviation.

C. Data Analysis

The general workflow, adopted for complete annotation of SCG waveforms, consists of two different phases as follows.

1) *Calibration:* In this phase, prototypes and parameters are extracted from calibration data, making use of both ECG and SCG recordings. Calibration is, in general, necessary in order to account for variations between patterns and relative amplitudes for different users. After calibration, the learned patterns and parameters may be reused, for the same subject, to perform SCG data annotation.
2) *Annotation:* This phase deals with identifying, in the test SCG waveforms only, the previously extracted patterns. Relevant feature points are recognized and marked in this phase, with the annotation procedure further breaking down to two stages. In the first stage, detection of heartbeat events is coarsely performed, exploiting a suitably defined signal (i.e., a *detection signal*). In the second stage, actual annotation of SCG is carried out, by trying to match the extracted prototype to the waveform being considered, around each detected heartbeat.

If only HR measurements are looked for, calibration can be self-consistently performed by taking an initial, quiet SCG period as a reference and by gathering statistics about the detection signal's local maxima: this provides a reliable enough frame for discriminating among beat complexes. If a more detailed annotation is needed, accounting for more landmarks in the SCG waveform, calibration avails itself of simultaneous acquisition of ECG potentials. This results in a simple, fully automated procedure, to be carried out just once per subject. In the following, for completeness' sake, the full methodology featuring extended calibration and annotation is described, with the following notation:

1) x_{DET}: the detection signal, used to coarsely locate heartbeats in the SCG;
2) x_{SCG}: the original SCG signal, to be annotated;
3) x_{PROTO}: the prototype of SCG patterns, extracted during the calibration phase.

1) Detection Signal: Detecting heartbeat events from SCG signals can be a difficult task, given the complexity of the pattern and superimposed noise: a simple thresholding approach is not a reliable option. This also holds somehow true for R peak detection within the ECG, where T waves may appear comparable in amplitude. Usually, isolating R peaks implies recognizing fast-varying signals, and methods based on derivatives are commonly employed. For instance, Arzeno *et al.* [33] compare several QRS-complex detection strategies exploiting suitably defined difference operators (in FIR form); [34] indicates second-derivative-based methods as a good compromise of sensitivity and computational efficiency. Taking a closer look at Fig. 1, several similarities can be noted between the detection of the fast-varying QRS complex and that of the MC–IM–AO one in the SCG. Therefore, the following signal is defined as a good proxy to detect cardiac beats within the SCG:

$$x_{\mathrm{DET,HF}} = \left(\frac{\partial^2 x_{\mathrm{SCG}}}{\partial t^2}\right)^3 \tag{2}$$

where the HF subscript indicates that this signal emphasizes high-frequency oscillations. In order to simplify further processing, a smoothed version of such signal is considered. One possible way for achieving this is by extracting the signal envelope by computing its analytic representation using the Hilbert transform. Another quick method is to filter the absolute value of $x_{\mathrm{DET,HF}}$

$$x_{\mathrm{DET}} = \mathrm{LPF}\left(\left|x_{\mathrm{DET,HF}}\right|\right) \tag{3}$$

where LPF is an FIR low-pass filter. Setting the cutoff frequency around 4 Hz was found to yield a good tradeoff between smoothness and preservation of temporal locality.

2) Calibration: Calibration is performed once per subject, based on the comparison between ECG and SCG signals. The former signal, in fact, is exploited to segment the latter one, in order to extract relevant information. As far as the ECG is concerned, QRS complexes are detected by exploiting second-order derivatives methods, as indicated in [33] and [34]; then, R peaks are easily marked. Once the R peaks locations are known, ensembles are constructed as follows.

1) For the beat detection signal x_{DET}, segments are extracted from a window $(t_{\mathrm{pre,DET}} - t_{\mathrm{post,DET}})$ with respect to each R peak (for this application example, $t_{\mathrm{pre,DET}} = -100$ ms, $t_{\mathrm{post,DET}} = 600$ ms). Local maxima of such windows are then marked and their values stored. Summary statistics are derived over this population; in particular, the 60th percentile is extracted as a threshold for subsequent reference beats detection, from now on named $A_{\mathrm{min,REF}}$.
2) For the SCG signal, x_{SCG}, segments are extracted from a window of $(t_{\mathrm{pre,SCG}} - t_{\mathrm{post,SCG}})$ with respect to each R peak (in this application context, $t_{\mathrm{pre,SCG}} = -50$ ms, $t_{\mathrm{post,SCG}} = 300$ ms). The resulting ensemble has dimensions (*beats* and *timesteps*). Median is then computed across all time instants, yielding a prototype waveform,

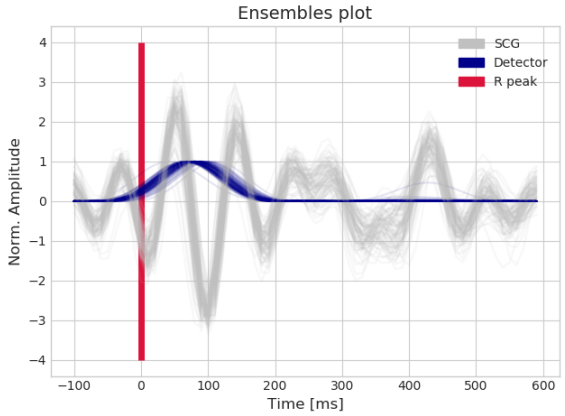

Fig. 4. Ensembles plot of SCG and detector signal. For clearer plotting, detector signals are normalized by *min–max* scaling.

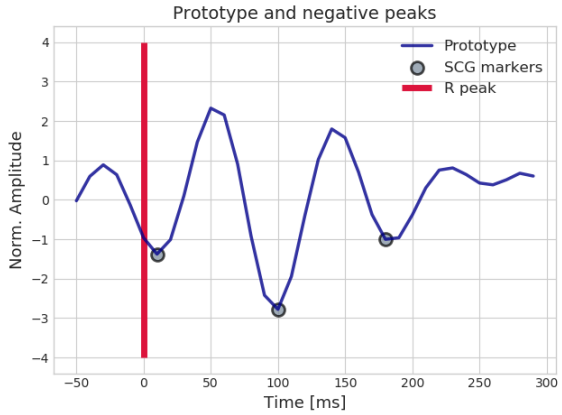

Fig. 5. Extraction of the prototype SCG signal, together with annotated fiducial points.

x_{PROTO} (whose length is *timesteps*), that will serve as template for matching candidate waveforms. Contextually, a set of reference negative peaks is marked, which will act as fiducial points in SCG annotation.

Fig. 4 shows an example of ensemble waveforms collected from a subject. For readability's sake, the detector signals were normalized to a (0–1) range using a simple *min–max* scaling approach: actual amplitudes are considered when computing the descriptive statistics. From the SCG waveforms in such an ensemble, the prototype is extracted and annotated, as shown in Fig. 5.

3) Heartbeat Detection: Heartbeat detection from SCG is performed by using the detector signal x_{DET} [defined in (3)], together with the statistical threshold $A_{\text{min,REF}}$ determined during calibration. At first, x_{DET} is scanned for local maxima: all peaks greater than $A_{\text{min,REF}}$ are taken as *reference peaks*. Then, leveraging this knowledge, peak-to-peak time intervals are computed, with the intent to discover possibly missing heartbeats. In this example, beat-to-beat intervals larger than 1.5 s (i.e., equivalent HR $\leq$ 40 bpm) are further processed. In order to estimate the number of missed beats (n_{MISS}) between two reference peaks, the mean from last five valid beat-to-beat intervals is used. Then, the top n_{MISS} peaks are found, imposing the following constraints.

Algorithm 1 Coarse Detection of Heartbeat Events

Inputs:

- x_{DET}: signal for heartbeat detection (on SCG data)
- $A_{\text{min,REF}}$: minimum amplitude for reference peaks

Begin:

Find reference peaks p such that $x_{\text{DET}}(p) \geq A_{\text{min,REF}}$
Compute beat intervals, detect too-long ones ($HR \leq HR_{LF}$ bpm)
ForEach interval **in** too-long intervals:
Estimate number of missing beats (n_{MISS})
Find n_{MISS} top peaks, such that:
- $HR_{LF} \leq HR \leq HR_{HF}$ bpm
- amplitude $\geq A_{\text{min,REF}}/4$
- if peaks are closer than T_{MIN}, choose first

Add interpolated peak to reference ones

Return index of possible heartbeats

1) Time between beats should fall within $[T_{\text{HF}} - T_{\text{LF}}]$ interval or in terms of HR between the equivalent $[\text{HR}_{\text{LF}} - HR_{\text{HF}}]$ range. In this application example (with no loss of generality), let us set $T_{\text{HF}} = 333$ ms, $T_{\text{LF}} = 1.5$ s, and consequently, $HR_{\text{LF}} = 40$ bpm, $HR_{\text{HF}} = 180$ bpm.
2) Beats should have an amplitude of at least $A_{\text{min,REF}}/4$.
3) If two comparable peaks are closer than T_{MIN} (in this example, 200 ms), choose the first one.

If no candidates are found, suitable for interpolation, the process gracefully logs the potential error and carries on the waveform analysis. On the other hand, each time new beats are found, they become knowledge base for future beats to be interpolated. The process of beat detection is reported as pseudocode in Algorithm 1.

4) SCG Waves Annotation: Once the heartbeat events are discovered, SCG annotation is performed. In order to do so, a window is extracted from x_{SCG} around each beat (in this application context, the window length is set to 500 ms). Within such window, the template x_{PROTO} (extracted at calibration phase) is best aligned to the signal x_{SCG} by maximizing a *cross correlation* metric. Finally, annotation of SCG local minima is performed on a basis of the minimum distance from the prototype's fiducial points. During annotation, it is possible that the algorithm is not able to match all reference points: nonetheless, the best guesses are logged, and information of such a partial match is stored too. In this way, the algorithm is more resilient and gracefully handles nonideal matches. The process of annotation is reported as pseudocode in Algorithm 2.

III. Results and Discussion

Before discussing the results in detail, it is worth delineating the scope of this paper, which aims at designing and testing specific solutions suitable for supporting A&HA policies. More specifically, this paper is framed into a more general vision, aimed at integrating into current prevention practices

Algorithm 2 SCG Waveform Annotation

Inputs:

- *detected beats*: array of beats indexes from Alg. 1
- x_{SCG}: SCG signal to annotate
- x_{PROTO}: SCG signal prototype, with fiducial points

Begin:

ForEach *beat* **in** *detected beats*:

Extract window $x_{\mathrm{SCG,W}}$ from x_{SCG}, centered around current *beat*

Align $x_{\mathrm{SCG,W}}$ to x_{PROTO} by maximizing cross correlation metric

Match x_{PROTO} and $x_{\mathrm{SCG,W}}$ local minima

Return indexes of matched points

tools for continuous monitoring of behavioral and clinical signs. Within this context, inexpensiveness, usability, and low intrusivity are of the utmost importance. Suitable tradeoffs should, therefore, be sought for, possibly differing from high-performance, fully featured clinical instruments. In particular, the current implementation looks forward to an embedded solution, in which multiple indicators will be assessed through the very same hardware device: eventually, the accelerometer sensor will be shared between heart and physical activity monitoring, carried out through a low-cost microcontroller platform. Constraints in power consumption and computational resources have therefore been taken into account in devising the overall strategy. For instance, a relatively low sampling frequency (100 Hz, namely) has been considered. This, of course, limits the accuracy when measuring short-time intervals, e.g., when evaluating PPT for blood pressure monitoring or when investigating specific, punctual rhythm anomalies. Nevertheless, the tool is not meant to substitute clinical-grade diagnostic instruments, but instead to discover trends and anomalies evaluated over a much longer time scale, which makes instant defects less significant. For the same reason, testing has been carried out on a healthy population, to address prevention strategies. Of course, evaluating the effectiveness of the proposed approach in terms of health outcomes would have required a much larger and longer trial: here, a functional, proof-of-concept validation is only given. The procedures for SCG annotation was applied in a completely automated framework, without any need for user intervention in setting parameters.

An example of output that the system produces is shown in Fig. 6. The top panel represents the filtered ECG signal, whose R peaks have been annotated (right-pointing yellow triangles). Immediately below, the detection signal x_{DET} is plotted: as a reference, the R peaks are also reported. It can be noted that the proposed method detects three reference beats (downward-pointing green triangles) and is able to correctly interpolate a missing one (the third, marked with an upward-pointing green triangle). Such information is then used to annotate the original SCG signal, shown in the bottom panel. Fiducial points are correctly identified (gray bullets), according to the extracted prototype in Fig 5.

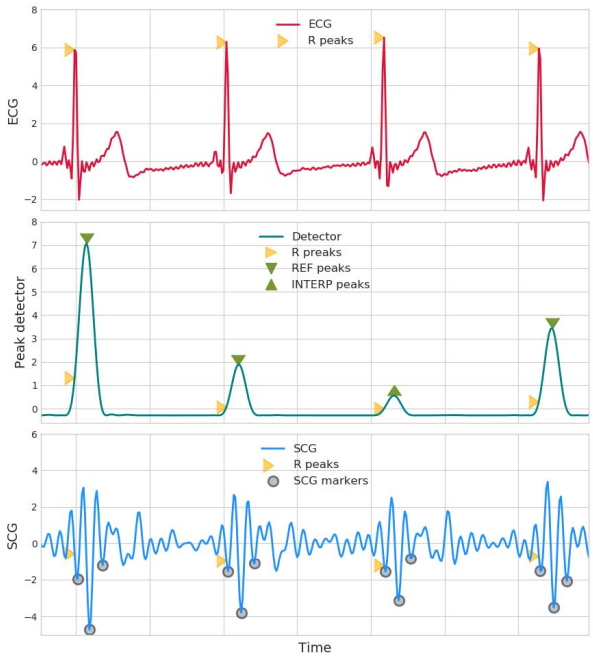

Fig. 6. Output of the annotation process. ECG and R peaks (left-pointing yellow triangles) (top). Beat detector signal, x_{DET}, with annotated reference and interpolated peaks (downward-pointing and upward-pointing green triangles, respectively) (center). SCG and annotated reference peaks (gray bullets) (bottom).

In order to assess the performance of the proposed methodology, three different metrics are monitored:

1) *Sensitivity* (or *True Positive Rate*), i.e., percentage of correctly identified heartbeats (compared to ECG)

$$\mathrm{Sens.} = \frac{\mathrm{TruePositives}}{\mathrm{TruePositives} + \mathrm{FalseNegatives}}. \tag{4}$$

2) *Precision*, defined as

$$\mathrm{Prec.} = \frac{\mathrm{TruePositives}}{\mathrm{TruePositives} + \mathrm{FalsePositives}}. \tag{5}$$

3) *Coefficient of variation* (R^2 score) between beat-to-beat intervals computed from ECG and SCG (taking one of its fiducial points as reference)

$$R^2 = 1 - \frac{\sum_i \left(t_{\mathrm{ECGi}} - \overline{t_{\mathrm{ECG}}}\right)^2}{\sum_i \left(t_{\mathrm{ECGi}} - \overline{t_{\mathrm{SCGi}}}\right)^2} \tag{6}$$

where t_{ECGi} is the ith beat-to-beat interval computed from ECG, t_{SCGi} is the SCG analogous, and $\overline{t_{\mathrm{ECG}}}$ is the average ECG beat-to-beat interval.

The R^2 metric, in particular, allows to assess the agreement between measures performed using SCG and the ECG gold standard, under the assumption of normal, nonaberrant beats: the good agreement shown allows for functionally validating the approach with reference to the aimed application target (namely, long-term monitoring in A&HA). Individual R^2, precision, and sensitivity scores, achieved in each session, are reported, for completeness' sake, in Table I; results are shown in two different split conditions:

1) *ALL*: all matched SCG patterns, i.e., partial and full matches;

TABLE I
RESULTS OF FULLY AUTOMATED SCG ANNOTATION

Record ID	Sens ALL	Sens FULL	Prec ALL	Prec FULL	R^2 ALL	R^2 FULL
1	77.5	64.0	96.6	95.9	0.666	0.988
2	91.0	86.1	100.0	100.0	0.995	0.994
3	92.7	80.9	100.0	100.0	0.968	0.963
4	80.4	79.7	100.0	100.0	0.934	0.935
5	98.1	98.1	100.0	100.0	0.996	0.996
6	83.5	80.0	100.0	100.0	0.963	0.961
7	86.5	86.5	91.8	91.8	0.938	0.938
8	94.3	94.3	97.8	97.8	0.932	0.932
9	91.6	91.6	100.0	100.0	0.996	0.996
10	95.5	95.5	100.0	100.0	0.996	0.996
11	100.0	100.0	100.0	100.0	0.994	0.994
12	95.6	89.5	97.3	97.1	0.899	0.982
13	97.4	97.4	100.0	100.0	0.996	0.996
14	96.0	96.0	100.0	100.0	0.998	0.998
15	90.4	90.4	100.0	100.0	0.99	0.99
Mean	91.4	88.7	98.9	98.8	0.951	0.977
Std	6.4	9.2	2.2	2.3	0.082	0.024

2) *FULL*: only fully matched SCG patterns.

On average, sensitivity scores of 88.7% and 91.4% were observed, for the *FULL* and *ALL* conditions, respectively: such difference in performance, due to more stringent requirements for a full match, is statistically significant ($p \approx 0.02$), as highlighted by a paired single-sided student test. Such scores are fairly comparable with other studies: in [35], for instance, a higher sensitivity figure (99%) is reported from measurements taken in lying positions and discarding approximately 6.6% of data, affected from motion artifacts, that is, such sensitivity is achieved on 93.4% of data, therefore, missing some beats as well. In this paper, instead, measurement is taken in sitting position (again to match the aimed application scenario), which is known to yield more contaminations than lying position [36]. Furthermore, no data are actually discarded at all, so that missing beats are mostly correlated with minor motion artifacts coming from sitting position. Taking into account such metric differences, performance figures well compares indeed. Furthermore, even though the annotation algorithm misses a beat, it logs such information: the previous beat-to-beat intervals are used to recognize anomalous values, due to a beat being skipped. Missing a beat every now and then does not jeopardize HR and HRV long-term monitoring: nevertheless, if missing a beat may imply losing relevant information (due to specific medical conditions) an increase in missing beat rate can be detected to trigger the caregiver attention and call for more accurate medical analysis. On the other hand, in terms of precision, the proposed method achieves high scores for both *ALL* and *FULL* conditions (without significant differences). Approximately, just 1% of identified peaks is, indeed, false positives: this may imply that detected ectopic (premature) beats are, indeed, actual beats.

Fig. 7 shows Bland–Altman plots relative to SCG–ECG beat-to-beat interval comparison. In such plot, the difference between two measures is displayed, with respect to their average: ideal agreement should look like all observations

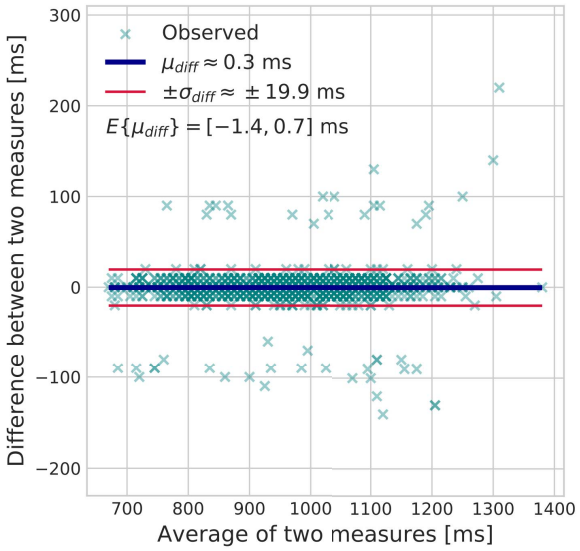

Fig. 7. Bland–Altman plot of all acquisitions. Mean difference (μ_{diff}) and standard deviation (σ_{diff}) are reported, along with the 95% confidence interval of the mean μ_{diff}. Note the different scales in the x- and y-axes.

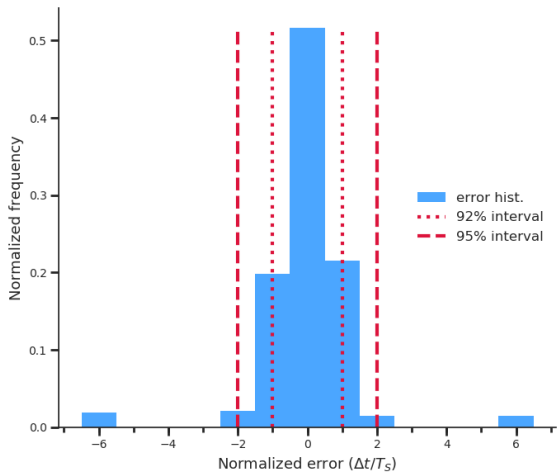

Fig. 8. Distribution of errors, normalized to the sampling period T_S. Over 92% of errors lies within $\pm 1\,T_S$, and the 95% HDPI is $\pm 2\,T_S$.

falling onto a straight horizontal line (the geometrical *locus* of the average of measures). The observed mean in difference μ_{diff} is approximately 0.3 ms, whereas its standard deviation σ_{diff} is 19.9 ms). These results were statistically analyzed; in particular, by applying student-t statistics, it is estimated that the 95% confidence interval of $E\{\mu_{\text{diff}}\}$ is (−1.4–0.7 ms): this implies a negligible bias error between the ECG and SCG measurements. As far as σ_{diff} is concerned, it is worth remarking that, in terms of sampling period (i.e., $T_S = 10\,ms$), its value corresponds to approximately two samples; furthermore, analysis of the distribution of such errors highlighted the presence of heavy tails that slightly inflate the σ_{diff} observed values. In particular, over 92% of errors lies within $\pm 1\,T_S$, whereas the 95% highest probability density interval (HDPI) is $\pm 2\,T_S$. This finding is shown in Fig. 8, reporting a histogram approximation of such errors Δt, normalized to T_S (and zoomed within $\pm 6\,T_S$ for clarity's sake). Therefore, errors are,

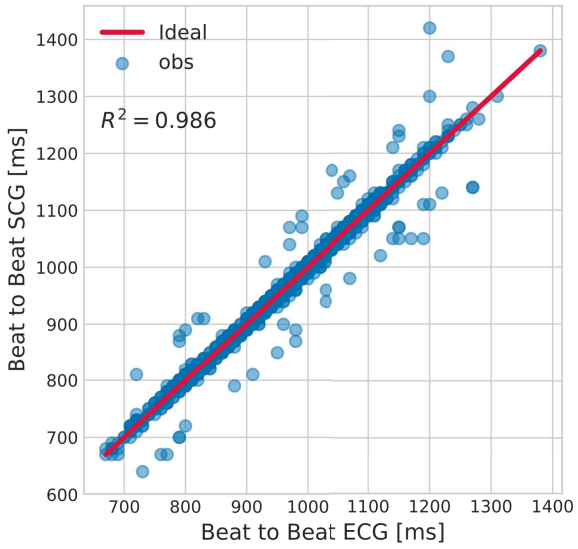

Fig. 9. Population-wide correlation plot between ECG (x-axis) and SCG (y-axis) beat-to-beat intervals. Red: ideal line representing perfect match. Blue: actual observed values.

in the vast majority, quite contained in terms of normalized time units.

Finally, a good average R^2 score is achieved in both *ALL* and *FULL* conditions (0.951 and 0.977, respectively, by averaging all different acquisitions). Despite slightly better results for the *FULL* condition, statistical analysis (paired, single-sided student test) does not highlight any significant difference between the two ($p \approx 0.12$), indicating good overall performance. High R^2 scores mean good agreement and linearity between the two measures performed with ECG and SCG. A population-wide correlation plot, obtained by considering all interbeat intervals, is shown in Fig. 9 (for the *FULL* condition): a value of 0.986 is observed. Such results are in line with recent works on public data sets [37]. In this case too, it is worth remarking that, with respect to mentioned studies, similar quality is attained in a somehow more challenging condition, due to: 1) the limitations coming from the low-cost and low-power constraints perspectively accounted for and 2) the test condition here referring to a sitting position, which is more prone to artifacts than supine lying case.

IV. Conclusion

This paper presented a fully automated procedure for acquiring SCG traces and for recognizing relevant heart patterns. The approach targets long-term monitoring in A&HA scenarios: inherent inexpensiveness, usability, and low intrusivity constraints are accounted for, while the approach is not meant to replace established medical devices, but to complement them instead. The procedure adapts itself to different users, by performing a preliminary calibration step, where information from ECG and SCG can be merged to derive detailed annotation parameters, if needed. Apart from such an optional, initial calibration phase, the system is fully self-consistent and no concurrent ECG acquisition is further needed. Analysis of SCG waveforms is broken down into two distinct phases. In the first one, a suitably engineered signal, based on second-order derivatives of the SCG, is exploited to coarsely locate heartbeat events. The second phase makes use of such information and performs actual annotation of SCG data, by comparing instants close to the detected heartbeats to a prototype, extracted during calibration.

The reliability of this annotation was assessed over different acquisition sessions by inspecting three main metrics: sensitivity (i.e., percentage of correctly identified heartbeats, compared to ECG), precision (i.e., the impact of false positives on truly detected beats), and R^2 (i.e., linearity between beat-to-beat measurements as computed by ECG and SCG). Results show very good performance: overall, nearly 90% of heartbeats are correctly detected, on average, with minimal false positives. Linearity between ECG and SCG-computed beat-to-beat intervals is extremely high ($R^2 > 0.95$, on average, and $R^2 > 0.97$, by considering fully matched samples only), indicating good agreement between the two measurement methods. SCG can thus be used as a reliable HR alternative, and favorably compares with other methods, such as PPG in [38]. Furthermore, SCG information can be profitably fused with other sources: if used in combination with ECG (as in the calibration setup) the system is able to measure other relevant quantities, including PEP and LVET: all such quantities are not measurable by other complementary techniques, such as PPG.

Another perspective advantage of monitoring SCG is that the same accelerometer sensor can be exploited for different purposes, with no further acquisition burden: for instance, physical activity intensity could be assessed [39], or gait quality parameters could be estimated. The approach is therefore quite promising, in view of more comprehensive, multidimensional behavioral monitoring in AAL environments.

References

[1] K. Mandula, R. Parupalli, C. Murty, E. Magesh, and R. Lunagariya, "Mobile based home automation using Internet of Things(IoT)," in *Proc. Int. Conf. Control, Instrum., Commun. Comput. Technol. (ICCICCT)*, Dec. 2015, pp. 340–343.

[2] G. Wilson *et al.*, "Robot-enabled support of daily activities in smart home environments," *Cognit. Syst. Res.*, vol. 54, pp. 258–272, Nov. 2018.

[3] R. Radziszewski, H. Ngankam, H. Pigot, V. Grégoire, D. Lorrain, and S. Giroux, "An ambient assisted living nighttime wandering system for elderly," in *Proc. 18th Int. Conf. Inf. Integr. Web-Based Appl. Services (iiWAS)*, 2016, pp. 368–374.

[4] C. Dobre, C. X. Mavromoustakis, N. M. Garcia, G. Mastorakis, and R. I. Goleva, "Introduction to the AAL and ELE systems," in *Ambient Assisted Living and Enhanced Living Environments*. Amsterdam, The Netherlands: Elsevier, 2017, pp. 1–16.

[5] N. Mora, I. De Munari, and P. Ciampolini, "Exploitation of a compact, cost-effective EEG module for plug-and-play, SSVEP-based BCI," in *Proc. 7th Int. IEEE/EMBS Conf. Neural Eng. (NER)*, Jul./Apr. 2015, pp. 142–145.

[6] N. Mora, V. Bianchi, I. D. Munari, and P. Ciampolini, "Controlling AAL environments through BCI," in *Proc. IEEE/ASME 10th Int. Conf. Mechatronic Embedded Syst. Appl. (MESA)*, Sep. 2014, pp. 1–6.

[7] N. Mora, G. Matrella, and P. Ciampolini, "Cloud-based behavioral monitoring in smart homes," *Sensors*, vol. 18, no. 6, p. 1951, Jun. 2018.

[8] C. Debes, A. Merentitis, S. Sukhanov, M. Niessen, N. Frangiadakis, and A. Bauer, "Monitoring activities of daily living in smart homes: Understanding human behavior," *IEEE Signal Process. Mag.*, vol. 33, no. 2, pp. 81–94, Mar. 2016.

[9] H. Al Osman, M. Eid, and A. El Saddik, "A pattern-based windowed impulse rejection filter for nonpathological HRV artifacts correction," *IEEE Trans. Instrum. Meas.*, vol. 64, no. 7, pp. 1944–1957, Jul. 2015.

[10] S. Mitra, M. Mitra, and B. B. Chaudhuri, "A rough-set-based inference engine for ECG classification," *IEEE Trans. Instrum. Meas*, vol. 55, no. 6, pp. 2198–2206, Dec. 2006.

[11] H.-Y. Tsai, K.-C. Huang, H.-C. Chang, J.-L. A. Yeh, and C.-H. Chang, "A noncontact skin oxygen-saturation imaging system for measuring human tissue oxygen saturation," *IEEE Trans. Instrum. Meas.*, vol. 63, no. 11, pp. 2620–2631, Nov. 2014.

[12] K. V. Madhav, R. M. Ram, E. H. Krishna, N. R. Komalla, and K. A. Reddy, "Robust extraction of respiratory activity from PPG signals using modified MSPCA," *IEEE Trans. Instrum. Meas.*, vol. 62, no. 5, pp. 1094–1106, May 2013.

[13] J. Tu and J. Lin, "Fast acquisition of heart rate in noncontact vital sign Radar measurement using time-window-variation technique," *IEEE Trans. Instrum. Meas.*, vol. 65, no. 1, pp. 112–122, Jan. 2016.

[14] S. Kazemi, A. Ghorbani, H. Amindavar, and D. R. Morgan, "Vital-sign extraction using bootstrap-based generalized warblet transform in heart and respiration monitoring radar system," *IEEE Trans. Instrum. Meas.*, vol. 65, no. 2, pp. 255–263, Feb. 2016.

[15] S. Bakhtiari *et al.*, "Compact millimeter-wave sensor for remote monitoring of vital signs," *IEEE Trans. Instrum. Meas.*, vol. 61, no. 3, pp. 830–841, Mar. 2012.

[16] X. He, R. A. Goubran, and X. P. Liu, "Secondary peak detection of PPG signal for continuous cuffless arterial blood pressure measurement," *IEEE Trans. Instrum. Meas.*, vol. 63, no. 6, pp. 1431–1439, Jun. 2014.

[17] M. D. Rienzo *et al.*, "Wearable seismocardiography: Towards a beat-by-beat assessment of cardiac mechanics in ambulant subjects," *Auton. Neurosci.*, vol. 178, nos. 1–2, pp. 50–59, 2013.

[18] M. D. Rienzo *et al.*, "Wearable seismocardiography for the beat-to-beat assessment of cardiac intervals during sleep," in *Proc. 36th Annu. Int. Conf. IEEE Eng. Med. Biol. Soc. (EMBC)*, Aug. 2014, pp. 6089–6091.

[19] M. Di Rienzo, E. Vaini, and P. Lombardi, "Development of a smart garment for the assessment of cardiac mechanical performance and other vital signs during sleep in microgravity," *Sens. Actuators A, Phys.*, vol. 274, pp. 19–27, May 2018.

[20] C.-S. Kim, A. M. Carek, O. Inan, R. Mukkamala, and J.-O. Hahn, "Ballistocardiogram-based approach to cuffless blood pressure monitoring: Proof of concept and potential challenges," *IEEE Trans. Biomed. Eng.*, vol. 65, no. 11, pp. 2384–2391, Nov. 2018.

[21] K. Lydon *et al.*, "Robust heartbeat detection from in-home ballistocardiogram signals of older adults using a bed sensor," in *Proc. 37th Annu. Int. Conf. IEEE Eng. Med. Biol. Soc. (EMBC)*, Aug. 2015, pp. 7175–7179.

[22] C. Yang, S. Tang, and N. Tavassolian, "Utilizing gyroscopes towards the automatic annotation of seismocardiograms," *IEEE Sensors J.*, vol. 17, no. 7, pp. 2129–2136, Apr. 2017.

[23] M. Mishra, H. Menon, and A. Mukherjee, "Characterization of S_1 and S_2 heart sounds using stacked autoencoder and convolutional neural network," *IEEE Trans. Instrum. Meas.*, to be published.

[24] A. Esmaili, M. Kachuee, and M. Shabany, "Nonlinear cuffless blood pressure estimation of healthy subjects using pulse transit time and arrival time," *IEEE Trans. Instrum. Meas.*, vol. 66, no. 12, pp. 3299–3308, Dec. 2017.

[25] F. Khosrow-Khavar, K. Tavakolian, A. P. Blaber, J. M. Zanetti, R. Fazel-Rezai, and C. Menon, "Automatic annotation of seismocardiogram with high-frequency precordial accelerations," *IEEE J. Biomed. Health Inform.*, vol. 19, no. 4, pp. 1428–1434, Jul. 2015.

[26] G. Shafiq, S. Tatinati, and K. C. Veluvolu, "Automatic annotation of peaks in seismocardiogram for systolic time intervals," in *Proc. 38th Annu. Int. Conf. IEEE Eng. Med. Biol. Soc. (EMBC)*, Aug. 2016, pp. 2672–2675.

[27] T. Choudhary, L. N. Sharma, and M. K. Bhuyan, "Automatic detection of aortic valve opening using seismocardiography in healthy individuals," *IEEE J. Biomed. Health Informat.*, to be published.

[28] D. M. Salerno and J. Zanetti, "Seismocardiography for monitoring changes in left ventricular function during ischemia," *CHEST J.*, vol. 100, no. 4, pp. 991–993, 1991.

[29] T. Hurnanen *et al.*, "Automated detection of atrial fibrillation based on time–frequency analysis of seismocardiograms," *IEEE J. Biomed. Health Informat.*, vol. 21, no. 5, pp. 1233–1241, Sep. 2017.

[30] O. Lahdenoja *et al.*, "Atrial fibrillation detection via accelerometer and gyroscope of a smartphone," *IEEE J. Biomed. Health Informat.*, vol. 22, no. 1, pp. 108–118, Jan. 2018.

[31] C. Guerra *et al.*, "The HELICOPTER project: A heterogeneous sensor network suitable for behavioral monitoring," (Lecture Notes in Computer Science) (Lecture Notes in Artificial Intelligence and Lecture Notes in Bioinformatics), vol. 9455. New York, NY, USA: Springer, 2015, pp. 152–163.

[32] S. Nunziata *et al.*, "IoT for active and healthy ageing: The ACTIVAGE DS-RER project," *Gerontechnology*, vol. 17, pp. 115–116, Apr. 2018.

[33] N. M. Arzeno, Z.-D. Deng, and C.-S. Poon, "Analysis of first-derivative based QRS detection algorithms," *IEEE Trans. Biomed. Eng.*, vol. 55, no. 2, pp. 478–484, Feb. 2008.

[34] J. S. Arteaga-Falconi, H. Al Osman, and A. El Saddik, "R-peak detection algorithm based on differentiation," in *Proc. IEEE 9th Int. Symp. Intell. Signal Process. (WISP)*, May 2015, pp. 1–4.

[35] M. Kaisti *et al.*, "Stand-alone heartbeat detection in multidimensional mechanocardiograms," *IEEE Sensors J.*, vol. 19, no. 1, pp. 234–242, Jan. 2019.

[36] G. Shafiq, S. Tatinati, W. T. Ang, and K. C. Veluvolu, "Automatic identification of systolic time intervals in seismocardiogram," *Sci. Rep.*, vol. 6, no. 1, p. 37524, Dec. 2016.

[37] S. Siecinski, P. S. Kostka, and E. J. Tkacz, "Heart rate variability analysis on CEBS database signals," in *Proc. 40th Annu. Int. Conf. IEEE Eng. Med. Biol. Soc. (EMBC)*, Jul. 2018, pp. 5697–5700.

[38] R.-C. Peng, X.-L. Zhou, W.-H. Lin, and Y.-T. Zhang, "Extraction of heart rate variability from smartphone photoplethysmograms," *Comput. Math. Methods Med.*, vol. 2015, 2015, Art. no. 516826.

[39] V. Bianchi *et al.*, "MuSA: A smart wearable sensor for active assisted living," in *Ambient Assisted Living* (Lecture Notes in Electrical Engineering), vol. 426. New York, NY, USA: Springer, 2017, pp. 197–208.

Niccolò Mora received the Electronic Engineering degree *(summa cum laude)* and the European Ph.D. degree (Doctor Europaeus) in information technologies from the University of Parma, Parma, Italy, in 2011 and 2015, respectively.

During his Ph.D. studies, he worked on the development of a compact, cost-effective BCI solution for active and assisted living systems control, part of which has been carried out in collaboration with the Defitech Foundation Chair in brain–machine interface at EPFL, Lausanne, Switzerland. His work A BCI Platform Supporting AAL Applications received a Best Paper Award at the International Human–Computer Interaction Conference (HCII) in 2014. He is currently an Associate Researcher with the Engineering and Architecture Department, University of Parma. His research activity is partly supported and framed within the Ambient Assisted Living (AAL) Joint Programme and the Horizon2020 Programme. His current research interests include Internet of Things (IoT)-enabled sensors development (hardware and software) to biosignal processing, with a particular focus on continuous monitoring of vital signs and daily life human behavioral patterns.

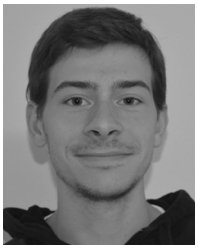

Federico Cocconcelli received the B.Sc. and M.Sc. degrees *(summa cum laude)* in electronic engineering from the University of Parma, Parma, Italy, in 2015 and 2018, respectively, where he is currently pursuing the Ph.D. degree in information technologies, under the supervision of Prof. P. Ciampolini.

His current research interests include cardiomechanical signals, noninvasive technologies for physiological parameters monitoring, sensors for smart living environments, and signal processing techniques.

Guido Matrella received the Electronic Engineering degree and the Ph.D. degree in information technology from the University of Parma, Parma, Italy, in 1999 and 2003, respectively.

Since 2007, he has been a Research Assistant with the University of Parma. He has worked in projects Radiation Active Pixel Sensor (RAPS) and Self-resetting High-gain Radiation Active Pixel Sensors (SHARPS), supported by the Italian National Institute for Nuclear Physics (INFN), in which innovative approaches aimed to optimize the use of standard technologies in specific contexts, such as experiments of high-energy physics (HEP), were devised. In the latest years, his main research activities are framed in the assistive technology field and, in particular, in the use of networks of smart sensors to elderly home behavior monitoring. Within this field, often called Ambient/Active Assisted Living (AAL), he participated in several European projects in the framework of AAL Joint Programme and Horizon2020. His current research interests include design of digital systems using hardware description language descriptions for integrated circuits and field-programmable gate arrays.

Paolo Ciampolini received the Electronic Engineering degree *(summa cum laude)* in electronic engineering and the Ph.D. degree in electronics and computer sciences in 1983 and 1989, respectively, from the University of Bologna, Bologna, Italy.

From 1990 to 1992, he was a Research Assistant with DEIS, University of Bologna. From 1992 to 1998, he was an Associate Professor with the University of Perugia, Perugia, Italy. From 1998 to 2001, he was an Associate Professor of electronics with the University of Parma, Parma, Italy, where he has been a Full Professor since 2001 and also an in charge of electronics fundamentals and digital design courses. From 2001 to 2008, he was the Chairman of the Board of Electronics with the Engineering Faculty, University of Parma. He is currently serving as technical/scientific coordinator of two projects funded in the framework of Ambient Assisted Living (AAL) Joint Programme. He has authored or coauthored more than 180 papers in technical journals or proceedings of international conferences. His current research interests include physical and numerical modeling of semiconductor devices, design and optimization of solid-state radiation sensors, digital circuit design, and assistive technology devices.